

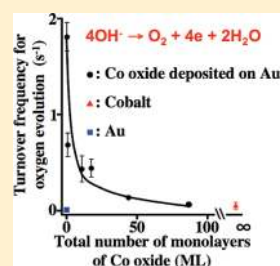
# Enhanced Activity of Gold-Supported Cobalt Oxide for the Electrochemical Evolution of Oxygen

Boon Siang Yeo and Alexis T. Bell\*

Chemical Sciences Division, Lawrence Berkeley National Laboratory, 1 Cyclotron Road, Berkeley, California 94720, United States  
Department of Chemical and Biomolecular Engineering, University of California—Berkeley, Berkeley, California 94720-1462, United States

 Supporting Information

**ABSTRACT:** Scanning electron microscopy, linear sweep voltammetry, chronoamperometry, and in situ surface-enhanced Raman spectroscopy were used to investigate the electrochemical oxygen evolution reaction (OER) occurring on cobalt oxide films deposited on Au and other metal substrates. All experiments were carried out in 0.1 M KOH. A remarkable finding is that the turnover frequency for the OER exhibited by  $\sim 0.4$  ML of cobalt oxide deposited on Au is 40 times higher than that of bulk cobalt oxide. The activity of small amounts of cobalt oxide deposited on Pt, Pd, Cu, and Co decreased monotonically in the order Au > Pt > Pd > Cu > Co, paralleling the decreasing electronegativity of the substrate metal. Another notable finding is that the OER turnover frequency for  $\sim 0.4$  ML of cobalt oxide deposited on Au is nearly three times higher than that for bulk Ir. Raman spectroscopy revealed that the as-deposited cobalt oxide is present as  $\text{Co}_3\text{O}_4$  but undergoes progressive oxidation to  $\text{CoO}(\text{OH})$  with increasing anodic potential. The higher OER activity of cobalt oxide deposited on Au is attributed to an increase in fraction of the Co sites present as  $\text{Co}^{\text{IV}}$  cations, a state of cobalt believed to be essential for OER to occur. A hypothesis for how  $\text{Co}^{\text{IV}}$  cations contribute to OER is proposed and discussed.



## 1. INTRODUCTION

The splitting of water either electrochemically or photoelectrochemically has the potential to provide a sustainable source of hydrogen for powering fuel cells, reducing  $\text{CO}_2$  to fuels (e.g.,  $\text{CH}_4$ ,  $\text{CH}_3\text{OH}$ ), and removing oxygen from biomass.<sup>1–3</sup> One of the key drawbacks to making these processes viable on an industrial scale is the inefficiency of available electrocatalysts for the oxygen evolution reaction (OER). This critical step occurs in acid via the reaction  $2\text{H}_2\text{O} \rightarrow 4\text{H}^+ + 4\text{e}^- + \text{O}_2$  and in base via the reaction  $4\text{OH}^- \rightarrow 2\text{H}_2\text{O} + 4\text{e}^- + \text{O}_2$ . The inefficiency of the catalyst is expressed in terms of the overpotential ( $\eta$ ) required above the standard reaction potential (1.23 V at pH = 0) in order to achieve a desired current density. Thus, to obtain a current density of  $10 \text{ mA/cm}^2$ , an overpotential of several hundred millivolts is often required. For this reason, extensive efforts have been undertaken to identify catalysts with low OER overpotentials.<sup>4–11</sup> While the oxides of Ru and Ir are considered to be the best OER catalysts for use in acid and base, respectively, these metals are among the rarest elements on earth and, hence, are not practical for large-scale applications. Cobalt, on the other hand, is earth-abundant and both  $\text{Co}_3\text{O}_4$  and the substituted cobaltites  $\text{M}_x\text{Co}_{3-x}\text{O}_4$  (M = Ni, Fe, or Cu) exhibit good OER activity.<sup>4,6,7,12,13</sup> For this reason, considerable effort has been devoted to the understanding of the changes in composition and structure of cobalt anodes as a function of applied potential and the influence of these changes on the rate of OER. Since Co and its oxides dissolve in acid, OER is performed in base.<sup>14</sup> Upon electrochemical oxidation, metallic Co

undergoes progressive oxidation to form  $\text{Co}(\text{OH})_2$ ,  $\text{CoO}$ ,  $\text{Co}_3\text{O}_4$ ,  $\text{CoO}(\text{OH})$ , etc.<sup>14–17</sup> Cyclic voltammograms of Co surfaces show an anodic peak at  $\sim 550 \text{ mV}$  (vs Hg/HgO reference) prior to the onset of oxygen evolution that has been assigned to the oxidation of  $\text{Co}^{\text{III}}$  to  $\text{Co}^{\text{IV}}$ .<sup>17–21</sup> This finding has led to the suggestion that  $\text{Co}^{\text{IV}}$  centers are required to catalyze OER. Such a view has recently been reinforced by ex situ electron paramagnetic resonance spectroscopy studies showing that the population of  $\text{Co}^{\text{IV}}$  species in a molecular cobalt–phosphate OER catalyst rises from 3 to 7% when the overpotential is increased from 326 to 526 mV during water oxidation.<sup>22</sup> It is also noteworthy that metal cations in high oxidation states have been proposed as active centers for OER catalysts based on the oxides of Mn, Ni, and Ir.<sup>5,21,23,24</sup>

The preceding discussion suggests that the efficiency of cobalt oxide as an OER catalyst could be enhanced by increasing the population of  $\text{Co}^{\text{IV}}$  centers present at the oxide surface. A possible way to achieve this goal would be to deposit a thin layer of cobalt oxide on the surface of a highly electronegative support such as Au. In support of this idea, density functional theory (DFT) calculations have shown that O binds more strongly to a monolayer of Co deposited on Au than to pure Co alone.<sup>25</sup> Hence, if chemisorbed oxygen is considered as a precursor to cobalt oxide formation, Co deposited on Au should be easier to oxidize than bulk Co. Further supporting this idea is a recent

Received: January 19, 2011

Published: March 17, 2011

report showing that 31 nm-diameter hollow spheres of  $\text{Co}_3\text{O}_4$  containing 14 nm-Au core nanoparticles are 2-fold more active for OER than equivalent particles of  $\text{Co}_3\text{O}_4$ .<sup>26</sup>

We report here the results of a systematic investigation of oxygen evolution catalyzed by cobalt oxide deposited onto the surface of electrochemically roughened Au. The structure of the cobalt oxide was characterized by scanning electron microscopy (SEM) and in situ surface-enhanced Raman spectroscopy (SERS). The electrochemical activity of cobalt oxide deposited on Au was determined from linear sweep voltammetry. To evaluate the effect of the support, cobalt oxide was also deposited onto Cu, Co, Pd, and Pt. The OER activity of a submonolayer of cobalt oxide decreases in the order of  $\text{CoO}_x/\text{Au} > \text{CoO}_x/\text{Pt} > \text{CoO}_x/\text{Pd} > \text{CoO}_x/\text{Cu} > \text{CoO}_x/\text{Co}$ . For comparison, OER experiments were also carried out with bulk Au, Cu, Co, Ir, Pd, and Pt electrodes. A remarkable finding of our work is that under equivalent electrochemical conditions, the OER activity of a  $\sim 0.4$  monolayer (ML) of cobalt oxide deposited on Au is roughly three times higher than that of bulk Ir and forty times higher than that of bulk cobalt oxide.

## 2. EXPERIMENTAL SECTION

Experimental details are given in Section S1 of the Supporting Information. In brief, electrochemical measurements were performed with a specially built Teflon cell designed for electrochemical studies and in situ Raman spectroscopy. The cell contains a circular working electrode (Au, Cu, Co, Ir, Pd, or Pt) with a geometric surface area of  $0.79 \text{ cm}^2$ . A Pt wire served as the counter electrode, and Hg/HgO was used as the reference electrode. Current–voltage curves were generated using a galvanostat/potentiostat. Potentials are reported with respect to the Hg/HgO reference electrode. The electrolyte used was 0.1 M KOH ( $\text{pH } 13.00 \pm 0.05$ ). Previous studies have shown that at this pH, Co does not dissolve.<sup>17,27</sup> In situ SER spectra of the electrodes were recorded during linear sweep voltammetry scans using a confocal Raman microscope coupled with a high numerical aperture water-immersion objective. A 633 nm laser was used to generate Raman spectra. The electrode surfaces and compositions were also examined by scanning electron microscopy (SEM) and energy dispersive spectroscopy (EDS). Prior to investigation, the Au anode was roughened electrochemically.<sup>28</sup> Cobalt oxide was deposited galvanostatically onto the roughened metal substrates from a cobalt nitrate/sodium acetate solution.<sup>29</sup> Cobalt oxide layers of  $\sim 0.4$ ,  $\sim 1$ ,  $\sim 11$ ,  $\sim 17$ ,  $\sim 44$ , and  $\sim 87$  ML (ML = monolayer equivalent, see Section S1 of Supporting Information) were deposited using anodic charges of 75, 170, 1900, 3000, 7500, and 15000  $\mu\text{C}$ , respectively.

## 3. RESULTS AND DISCUSSION

### 3.1. Characterization of Cobalt Oxide Deposited on Gold.

Figure 1 shows SEM images of roughened Au anodes deposited with increasing larger amounts of cobalt oxide. The images of clean Au and one that is coated with  $\sim 0.4$  ML cobalt oxide (Figure 1a and 1b) are very similar in appearance. Well-defined nanoparticles are observed with diameters of 50–200 nm. As the thickness of cobalt oxide increases, the appearance of the Au nanoparticles becomes progressively hazy (Figure 1c and 1d). This phenomenon is attributed to the presence of the nonconducting cobalt oxide deposited uniformly over the Au surface. This effect is most clearly seen in Figure 1e, for which the deposit corresponds to  $\sim 87$  ML cobalt oxide. In this case, the cobalt oxide shell is 25 nm thick. Energy dispersive spectroscopy (EDS) performed on the sample position (marked with the white X)

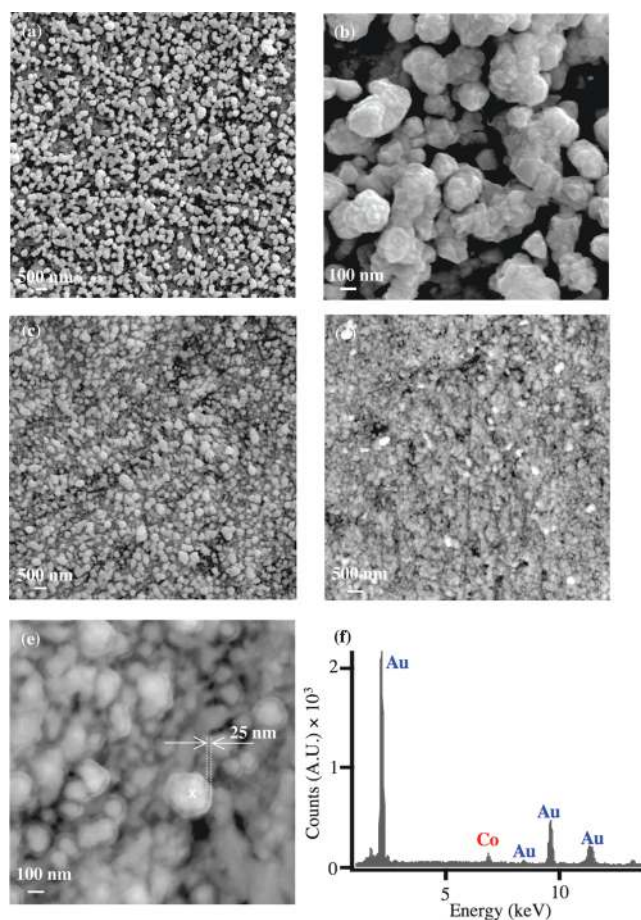


**Figure 1.** Scanning electron micrographs of electrochemically roughened Au surfaces coated with (a)  $\sim 0.4$  ML of cobalt oxide, (b)  $\sim 0.4$  ML of cobalt oxide (a higher magnification of Figure 1a), (c)  $\sim 44$  ML of cobalt oxide, and (d)  $\sim 87$  ML of cobalt oxide. (e) A higher magnification of Figure 1d reveals that each Au nanoparticle is surrounded by a cobalt oxide halo of  $\sim 25$  nm. (f) The energy dispersive spectrum taken at the spot marked with the white X in Figure 1(e).

confirms the presence of cobalt (Figure 1f). EDS-elemental analysis maps showed that the cobalt oxide was uniformly distributed across the Au support, and no evidence for the formation of cobalt oxide islands was found in any of the SEM images collected (Section S2 of the Supporting Information). For deposits of more than 1 ML, the as-deposited cobalt oxide was identified as  $\text{Co}_3\text{O}_4$  (Section S3 of the Supporting Information).

**3.2. Oxygen Evolution Reaction Activity of  $\text{CoO}_x/\text{Au}$ .** The oxygen evolution activity of Au anodes with various thicknesses of cobalt oxide was measured in 0.1 M KOH. Similar measurements for pure Co and Au electrodes were also performed. Figure 2a shows linear sweep voltammetry (LSV) curves of the  $\sim 0.4$  ML cobalt oxide/Au (black trace), pure Au (blue), and pure Co (red). A theoretical curve (dotted) constructed by simple addition of currents contributed by pure Au and the equivalent of  $\sim 0.4$  ML of cobalt oxide, corresponding to  $6.98 \times 10^{14}$  surface Co atoms, is also included. This curve is an approximation to the anodic currents that would be obtained assuming that Au does not affect the OER activity of the adsorbed cobalt oxide, and vice versa. The large difference in anodic currents of this curve compared with that for  $\sim 0.4$  ML

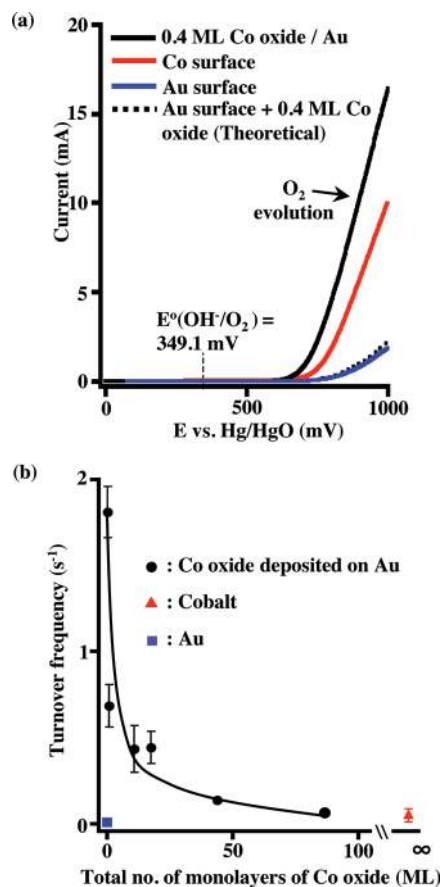


**Figure 2.** (a) Experimental linear sweep voltammetry curves of the  $\sim 0.4$  ML cobalt oxide/Au system, pure Au (electrochemically determined surface area =  $2.9 \text{ cm}^2$ , surface Au atoms =  $4.4 \times 10^{15}$ ) and pure Co ( $34.6 \text{ cm}^2$ , surface Co atoms =  $2.1 \times 10^{16}$ ) electrodes in  $0.1 \text{ M KOH}$ . The curves are scanned at  $1 \text{ mV/s}$ . A theoretical curve composed of a linear addition of currents taken from pure Au (blue trace) + amount of current that would be contributed by  $6.98 \times 10^{14}$  surface Co atoms (derived from the red curve) is also included. (b) A plot of turnover frequencies of the different cobalt oxide/Au electrodes (evaluated at a potential of  $700 \text{ mV}$ ) vs the number of monolayers of cobalt oxide present. The TOFs for pure Co and Au are also included in this plot.

cobalt oxide/Au clearly shows that Au does affect the activity of the deposited cobalt oxide.

The OER activities of the different electrodes were evaluated at a potential of  $700 \text{ mV}$  ( $\eta = 351 \text{ mV}$ ). The currents obtained at this potential were converted to turnover frequencies (TOFs) (Section S4 of the Supporting Information). The TOF plotted as a function of the number of monolayers of cobalt oxide molecules deposited on Au is shown in Figure 2b. The TOFs for pure Co and Au are also included in this plot. It should be noted that the TOF is calculated on the basis of number of surface Co or Au atoms for all cases, except for  $\sim 0.4 \text{ ML}$  and  $\sim 1.0 \text{ ML}$  cobalt oxide/Au, for which the total number of deposited cobalt atoms were used.

It is evident that the TOFs of the cobalt oxide/Au electrodes decrease rapidly as the thickness of the cobalt oxide deposit increases. The  $\sim 0.4 \text{ ML}$  cobalt oxide/Au sample exhibits the highest TOF,  $\sim 1.8 \text{ s}^{-1}$ , which is more than 1 order of magnitude higher than that for  $\sim 87 \text{ ML}$  of cobalt oxide/Au,  $6 \times 10^{-2} \text{ s}^{-1}$ . The TOF for Au is  $7 \times 10^{-3} \text{ s}^{-1}$  and that for pure Co is

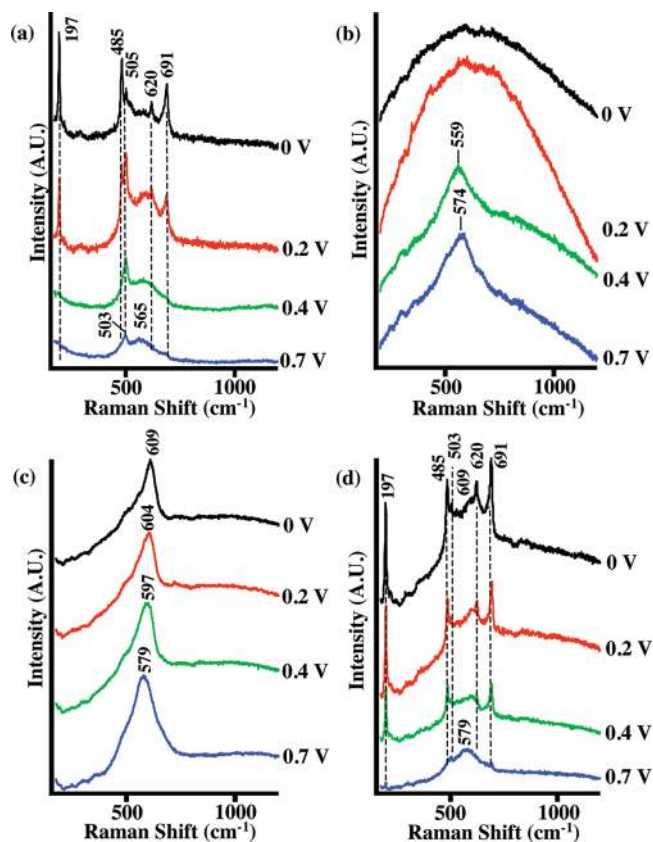


**Figure 3.** In situ Raman spectra of (a) Co surface, (b) Au, (c)  $\sim 0.4 \text{ ML}$  cobalt oxide/Au, and (d)  $\sim 87 \text{ ML}$  cobalt oxide/Au in  $0.1 \text{ M KOH}$ . All the spectra were collected in real time during linear sweep voltammetry scans at  $2 \text{ mV s}^{-1}$ . The acquisition times for the surface-enhanced and normal Raman spectra are 5–6 and 15 s, respectively.

$5.0 \times 10^{-2} \text{ s}^{-1}$ , in good agreement with values reported previously,  $6.0 \times 10^{-3} \text{ s}^{-1}$  to  $2.0 \times 10^{-2} \text{ s}^{-1}$ .<sup>4,6</sup> It is also noted that the TOFs for  $\sim 87 \text{ ML}$  of cobalt oxide/Au and bulk Co are virtually the same, which demonstrates that the electrochemical behavior of a thick cobalt oxide layer deposited on Au is similar to that of a bulk Co electrode.

**3.3. In Situ Raman Spectroscopy of  $\text{CoO}_x/\text{Au}$ .** The in situ Raman spectra of Au, Co, and Au on which  $\sim 0.4 \text{ ML}$  and  $\sim 87 \text{ ML}$  of cobalt oxide were deposited are shown in Figure 3. All spectra were acquired in  $0.1 \text{ M KOH}$  during a linear voltammetry scan from 0 to  $1.0 \text{ V}$ . For a pure Co surface, peaks are observed at  $197, 485, 620,$  and  $691 \text{ cm}^{-1}$  at  $0 \text{ V}$  (Figure 3a). These features are respectively assigned to the  $F_{2g}$ ,  $E_g$ ,  $F_{2g}$ , and  $A_{1g}$  vibrational modes of spinel-type  $\text{Co}_3\text{O}_4$ , which is expected to be thermodynamically stable in  $0.1 \text{ M KOH}$  at  $0 \text{ V}$ .<sup>14,30,31</sup> The sharp peak at  $505 \text{ cm}^{-1}$  is ascribed to  $\text{CoO}(\text{OH})$ , based on the observation of a similar peak in the Raman spectrum of bulk  $\text{CoO}(\text{OH})$ .<sup>30,32</sup> The formation of  $\text{Co}^{\text{III}}$  oxide on the surface of  $\text{Co}_3\text{O}_4$  is consistent with the interpretation of electrochemical data made by Conway and Liu.<sup>33</sup> As the potential is raised toward  $0.7 \text{ V}$ , the potential at which OER occurs, the peaks belonging to  $\text{Co}_3\text{O}_4$  gradually attenuate and two new features appear at  $503$  and  $565 \text{ cm}^{-1}$ . These two bands are ascribed to  $\text{CoO}(\text{OH})$ .<sup>17,30,32</sup> Spectra were also collected at  $>0.8 \text{ V}$  using a long working distance objective because  $\text{O}_2$  bubbling prevented the use of the more efficient water-immersion objective. The spectrum obtained in this case



(see Figure S5) resembles that taken at 0.7 V, but exhibits an even sharper band at  $503\text{ cm}^{-1}$ . These results indicate that under conditions of OER, the surface of a Co electrode is covered largely by  $\text{CoO}(\text{OH})$ . No evidence was found for a well-defined  $\text{Co}^{\text{IV}}$  oxide phase. The coexistence of  $\text{Co}^{\text{III}}$  and  $\text{Co}^{\text{IV}}$  has been reported, though, based on in situ Mössbauer spectroscopy observations of Co polarized at a  $\eta = 318\text{ mV}$  for OER.<sup>34,35</sup> Additionally, in situ X-ray absorption near-edge structure spectroscopy (XANES) characterization of a cobalt water oxidation catalyst deposited from a cobalt phosphate solution has shown that as the potential was raised to a level above the onset for OER, the apparent oxidation state of Co increased to above  $3+$ .<sup>36</sup>

In the case of a Au anode, oxide formation was not observed for potentials  $\leq 0.2\text{ V}$  (Figure 3b). The elevated spectral background is associated with high SERS activity exhibited by the metal surface and can be attributed to photons emitted during the annihilation of inelastically scattered localized surface plasmons.<sup>37</sup> At  $0.4\text{ V}$ , a feature appears at  $\sim 559\text{ cm}^{-1}$ , which blue shifts with increasing potential to  $\sim 574\text{ cm}^{-1}$ . This feature is assigned to the Au–O stretching vibration of Au oxide.<sup>28</sup> The blue shift in the frequency of this band with increasing potential has been observed previously in our own studies and those of Weaver et al.<sup>28,38</sup>

For  $\sim 0.4\text{ ML}$  of cobalt oxide deposited on Au, a sharp band at  $609\text{ cm}^{-1}$  was observed at  $0\text{ V}$  (Figure 3c). As the potential was increased, the entire band monotonically red-shifted to  $579\text{ cm}^{-1}$ , suggesting that most if not all of the surface species are oxidized collectively (otherwise a doublet would have been observed). This band is ascribed to presence of dispersed  $\text{CoO}_x$  species on the surface of the Au anode. Interestingly, no feature was observed for  $\text{AuO}_x$ , which is what would have been expected if the Co were present as small particles rather than being uniformly distributed. The attribution of the band at  $579\text{--}609\text{ cm}^{-1}$  to cobalt oxide is supported by the observation of a feature in this region for  $\text{CoO}_x$  highly dispersed on the zeolite ZSM5.<sup>39</sup> The increase in the vibrational frequency at higher potentials is attributed to the oxidation of the  $\text{Co}^{\text{II}}$  and  $\text{Co}^{\text{III}}$  toward  $\text{Co}^{\text{IV}}$  and is supported by the following observations: In situ Raman studies of the electrochemical oxidation of  $\text{LiCoO}_2$  to  $\text{Li}_{1-x}\text{CoO}_2$  have shown that as Li is progressively removed and the oxidation state of Co increases toward  $4+$ , the Raman bands of  $\text{LiCoO}_2$  at  $596\text{ cm}^{-1}$  ( $x = 0$ ) red-shifts to  $572\text{ cm}^{-1}$  ( $x = 0.6$ ).<sup>40</sup> The Raman band of  $\text{CoO}_x$  species deposited in an  $\text{O}_2/\text{Ar}$  plasma has also been found to decrease from  $597$  to  $530\text{ cm}^{-1}$  as the mole fraction of  $\text{O}_2$  in the plasma increased.<sup>41</sup> The assignment of the band at  $579\text{--}609\text{ cm}^{-1}$  to other forms of cobalt oxides, e.g.,  $\text{CoO}$ ,  $\text{Co}(\text{OH})_2$ ,  $\text{CoO}(\text{OH})$ ,  $\text{Co}_3\text{O}_4$ , can be ruled out because the spectra of these oxides do not contain bands in this range.<sup>30,31</sup> Similarly, this feature cannot be assigned to the  $\nu(\text{Au}\text{--}\text{O})$  of Au oxide because the frequency of the latter shifts to higher values with increasing potential.

The Raman spectrum of a Au anode containing  $\sim 87\text{ ML}$  of cobalt oxide exhibits features that are similar to those seen in the spectra of bulk Co and of Au onto which  $\sim 0.4\text{ ML}$  cobalt oxide had been deposited (Figure 3d). At  $0\text{ V}$ , the principle bands are those assignable to  $\text{Co}_3\text{O}_4$ . Progressive electrochemical oxidation results in the oxidation of  $\text{Co}_3\text{O}_4$  to  $\text{CoO}(\text{OH})$  ( $503\text{ cm}^{-1}$ ). The feature appearing at  $579\text{ cm}^{-1}$  is attributed to  $\text{CoO}_x$  species. In accordance with the discussion above, the  $\text{CoO}_x$  must lie adjacent to the Au substrate (verified by the strong intensity of its  $579\text{ cm}^{-1}$  band as result of SERS enhancement from the proximate Au substrate).<sup>42</sup>

The possibility that the  $579\text{--}609\text{ cm}^{-1}$  band is due to residual species in the plating solution from which Co oxide was electro-deposited can be ruled out, since the electrode was washed thoroughly after cobalt oxide deposition. This is further verified by comparing the frequency of this band with those of cobalt nitrate and sodium acetate (Section S6 of Supporting Information).

**3.4. OER Activity of  $\text{CoO}_x/\text{M}$  ( $\text{M} = \text{Au}, \text{Pt}, \text{Pd}, \text{Cu}$ ).** The mechanism for the electrochemical oxidation of water at a Co anode in base is not fully understood. Nevertheless, the general consensus is that with increasing anodic potential, the surface of Co undergoes progressive oxidation, and that  $\text{Co}^{\text{IV}}$  species, formed at potentials where oxygen evolution occurs, are essential intermediates in the evolution of  $\text{O}_2$ .<sup>17–21</sup> These conclusions suggest that the enhanced OER activity of cobalt oxide deposited on Au may be due to an increase in the oxidation of the deposited oxide caused by the Au. In support of this interpretation we note that since Au is the most electronegative transition metal, it could act as an electron sink to facilitate the oxidation of  $\text{Co}^{\text{II}}$  and  $\text{Co}^{\text{III}}$  in cobalt oxide to  $\text{Co}^{\text{IV}}$ . Evidence for the transfer of electronic charge from  $\text{SnO}_2$  to Au has also been observed by X-ray photoelectron spectroscopy of a  $\text{Au}@/\text{SnO}_2$  core/shell catalyst, which was shown to be more active for the oxidation of CO than  $\text{SnO}_2$  alone.<sup>43</sup> Another indicator that the deposition of Co on Au can promote the oxidation of Co comes from quantum chemical studies, which have shown that O atoms are more strongly bound to a monolayer of Co deposited on Au than on Co.<sup>25,44</sup> This effect has been attributed to the tensile strain exerted by the Au support on the Co overlayer, which causes the d-band center of Co to increase in energy and in turn the Co–O binding energy.

To evaluate the above hypothesis, the OER activity was measured for  $75\text{ }\mu\text{C}$  of cobalt oxide deposited onto Au, Pt, Pd, and Cu anodes. This is equivalent to  $\sim 0.4\text{ ML}$  for the Au surface. The OER activities of pure Au, Pt, Pd, and Cu were also measured for comparison. Since it is not possible to roughen all the surfaces to the same degree, only mechanically polished metal surfaces were used. The LSV curves of the pure metal substrates were measured from  $0$  to  $1\text{ V}$ . They were then reduced potentiostatically and rinsed in water, after which  $75\text{ }\mu\text{C}$  of cobalt oxide was deposited galvanostatically onto the surface of each metal. The LSV curve was then remeasured in  $0.1\text{ M KOH}$ .

As seen in Figure 4, deposition of  $75\text{ }\mu\text{C}$  of cobalt oxide onto Pt, Pd, and Cu resulted in a higher OER activity than that measured on the bare metal (the data for the Au system are similar to those shown in Figure 2a and therefore are not included in Figure 4). The only exception was Co, for which deposition of  $75\text{ }\mu\text{C}$  of cobalt oxide had no effect on the OER activity of Co observed in the absence of the deposit. This experiment assured that the changes in faradaic currents were not artifacts arising from residual Co plating solutions.

The TOFs for OER at an applied potential of  $700\text{ mV}$  for  $75\text{ }\mu\text{C}$  of cobalt oxide deposited on Au, Pt, Pd, Cu, and Co are compared in Figure 5. The TOF in each case was determined in the same manner as that done for cobalt oxide deposited on Au (Section S4 of Supporting Information). Also shown in this figure are values of the electronegativity for each metal and the Co–O binding energy for a monolayer of Co deposited on each metal.<sup>25</sup> The TOF for oxygen evolution clearly depends on the composition of the metal supporting the cobalt oxide deposited and decreases in the order  $\text{Au} > \text{Pt} > \text{Pd} > \text{Cu} > \text{Co}$ . It is also evident that the TOF decreases with decreasing electronegativity of the underlying metal and with the binding energy of the Co–O bond.

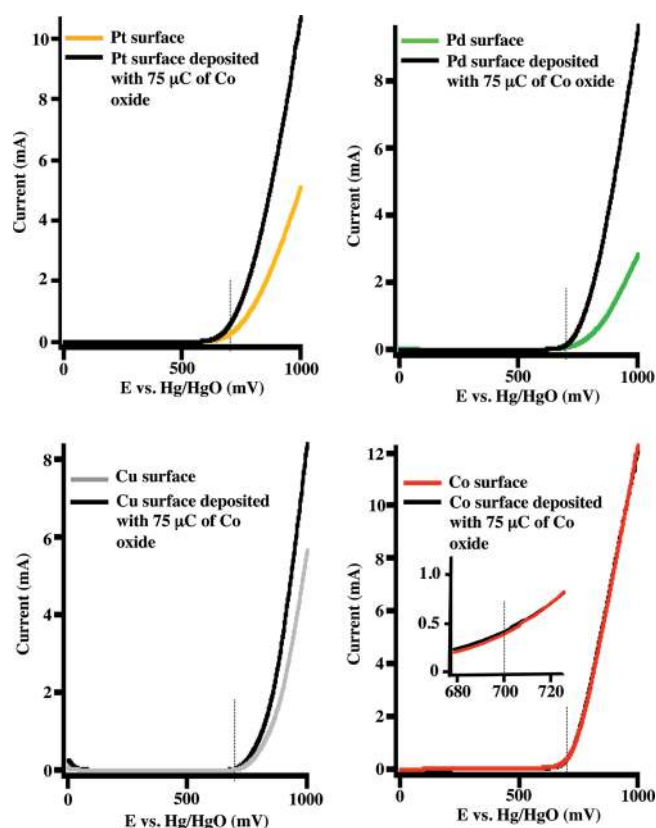


**Figure 4.** Linear sweep voltammetry curves of various metal electrodes in 0.1 M KOH. The scans are taken at 1 mV/s. A blow-up of the LSV curves of Co is included. The dotted line marks 700 mV.

It is also interesting to compare the TOFs of all the anodes investigated in this study. The results presented in Table 1 were obtained under identical conditions. For reference, we have included the TOF for pure Ir (see Section S7 of Supporting Information), since this metal has been reported to be the most active for the OER in basic electrolyte.<sup>23</sup> Our measurements of the TOFs for metal anodes show that the activity decreases in the order  $\text{Ir} \gg \text{Co} > \text{Pt} > \text{Pd} > \text{Cu} > \text{Au}$ . This qualitative trend agrees with previously published studies.<sup>45–49</sup> For example, at  $\eta = 350$  mV, the current density of Ir in 25% KOH has been reported to be approximately 10-fold higher than that of Pt.<sup>50</sup> This ratio is consistent with that seen in Table 1 for Ir compared to Pt. Table 1 also demonstrates that  $\sim 0.4$  ML of cobalt oxide deposited on Au is about three times more active than pure Ir, and that activities comparable to that of Ir can be achieved for 75  $\mu\text{C}$  of cobalt oxide deposited on Pt and about 1.0 ML of cobalt oxide deposited on Au.

To assess the stability of the cobalt oxide-modified Au electrode, chronoamperometry measurements were performed on the  $\sim 0.4$  ML cobalt oxide/Au electrode at 0.75 V over 18 h (see Section S8 of Supporting Information). For comparison, similar measurements were made on Co, Au, and Ir electrodes. The steady-state OER current density of the  $\sim 0.4$  ML cobalt oxide/Au electrode was found to be highly stable and shows no sign of degradation even over 18 h. Thus, the results of the present investigation indicate that submonolayer deposits of cobalt oxide on Au are superior catalysts to Ir for the electrochemical evolution of  $\text{O}_2$  in basic electrolyte and are stable with prolonged use.

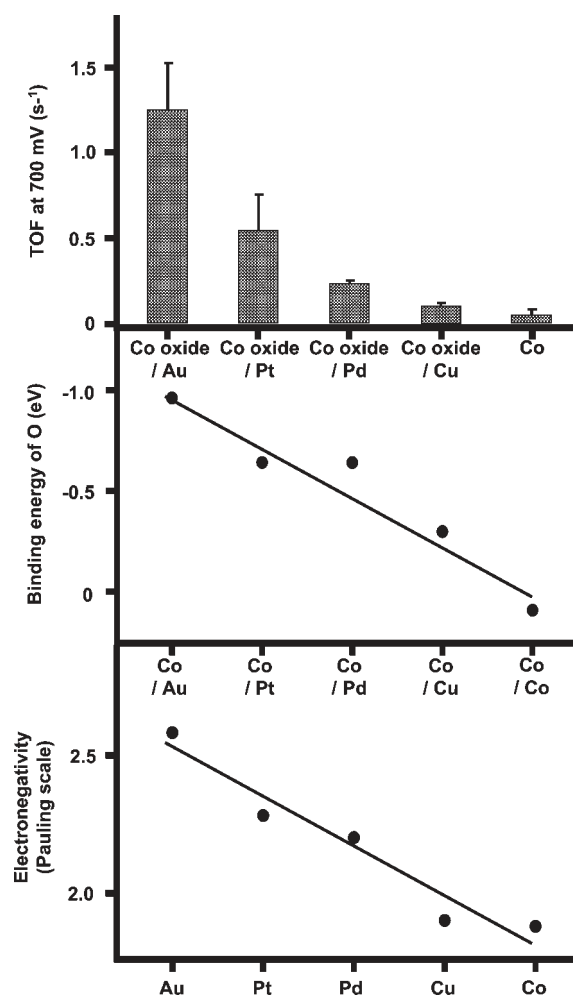


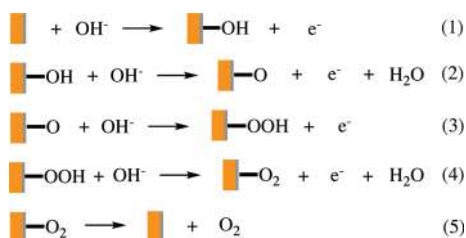
**Figure 5.** A histogram plot of the turnover frequencies of 75  $\mu\text{C}$  cobalt oxide deposited on smooth Au, Pt, Pd, and Cu. The value for Co is also included. The electronegativity of the underlying support as well as the oxygen binding energies of the O–Co/M are also plotted out.

As noted earlier, the cumulative evidence from the literature suggests that OER occurs on a cobalt oxide layer formed on the surface of metallic Co and that under conditions of OER the oxide is best described as OER-inactive  $\text{CoO}(\text{OH})$ -containing OER-active  $\text{Co}^{\text{IV}}$  cations.<sup>17,33–35</sup> The formation of  $\text{CoO}(\text{OH})$  is well supported by the in situ Raman spectra reported here. While direct evidence for  $\text{Co}^{\text{IV}}$  cation was not found in the present study, we attribute the enhanced activity of thin cobalt oxide layers deposited on Au to the role of Au in facilitating the oxidation of Co, thereby raising the concentration of  $\text{Co}^{\text{IV}}$  cations present at the cobalt oxide surface at a given applied potential.

To address the question of why  $\text{Co}^{\text{IV}}$  cations are needed to enable OER, it is useful to consider the reaction mechanism shown in Figure 6, which has been adapted from the work of Lyons and Brandon for Co and Nørskov and co-workers for  $\text{RuO}_2$  and  $\text{TiO}_2$ .<sup>21,51</sup> In this scheme, reaction begins with the adsorption and discharge of  $\text{OH}^-$  anion at the anode surface to form adsorbed OH species (reaction 1). This step is followed by the reaction of  $\text{OH}^-$  with the adsorbed OH species to produce  $\text{H}_2\text{O}$  and adsorbed atomic O and the release of an electron (reaction 2). The third step in the sequence (reaction 3) involves

**Table 1. Average Turnover Frequencies at 700 mV of the Various Metal Electrodes Studied in This Work**

substrate	amounts of cobalt oxide deposited	average turnover frequency (s <sup>-1</sup> )
roughened Au substrate	~0.4 ML cobalt oxide	1.81
	~1.0 ML cobalt oxide	0.68
	~11 ML cobalt oxide	0.43
	~17 ML cobalt oxide	0.44
	~44 ML cobalt oxide	0.14
	~87 ML cobalt oxide	0.063
metal substrate	75 μC cobalt oxide/Au	1.24
	75 μC cobalt oxide/Pt	0.55
	75 μC cobalt oxide/Pd	0.22
	75 μC cobalt oxide/Cu	0.10
Ir	N.A.	0.64
Co	N.A.	0.047
Pt	N.A.	0.033
Pd	N.A.	0.024
Cu	N.A.	0.0155
Au	N.A.	0.0071

**Figure 6.** A schematic diagram depicting the mechanism for electrochemical oxygen evolution reaction on cobalt oxide/Au. The cobalt oxide (gray) overlayer is above the Au support (gold).

the reaction of an OH<sup>-</sup> anion with an adsorbed O atom to form adsorbed OOH species, which then undergo reaction with additional OH<sup>-</sup> anions (reaction 4), resulting in the formation of adsorbed O<sub>2</sub> and H<sub>2</sub>O and the release of an electron. Adsorbed O<sub>2</sub> then desorbs in the last step of the sequence (reaction 5). The rate-limiting step is hypothesized to be reaction 3. We postulate that Co<sup>IV</sup> cations enhance the electrophilicity of the adsorbed O, thereby facilitating the formation of O–OH via nucleophilic attack by an incoming OH<sup>-</sup> anion with an O atom associated with Co<sup>IV</sup>. The Co<sup>IV</sup> cations are also likely to promote the deprotonation of the OOH species, via electron-withdrawing inductive effect, to form O<sub>2</sub>.

#### 4. CONCLUSION

A combination of scanning electron microscopy, linear sweep voltammetry, chronoamperometry, and in situ surface-enhanced Raman spectroscopy was used to investigate the oxygen evolution reaction (OER) occurring on the surface of cobalt oxide supported on various metal substrates. The turnover frequency (TOF) for the OER occurring on a submonolayer of cobalt oxide deposited on Au (~1.8 s<sup>-1</sup>) is nearly 40 times higher than that of bulk Co (~0.05 s<sup>-1</sup>), and decreases monotonically to that of bulk Co as the thickness of the cobalt oxide deposit increases. For oxide deposits of more than 1.0 ML, Raman spectroscopy shows

that as-deposited cobalt oxide is present as Co<sub>3</sub>O<sub>4</sub>. With increasing anodic potential this compound is oxidized to CoO(OH). It is observed as well that for similar amounts of cobalt oxide deposited on Pt, Pd, Cu, and Co, the TOF for the OER decreases monotonically in the order Au > Pt > Pd > Cu > Co. A further finding of this study is that the activity of 0.4 ML cobalt oxide deposited on Au is nearly three times higher than that of Ir under identical reaction conditions. The enhancement in electrochemical activity of cobalt oxide deposited on Au is attributed to the increase in surface Co<sup>IV</sup> population as a result of enhanced oxidation of the cobalt oxide mediated by the Au support. To our knowledge, this work provides the first systematic study of how metals can be used to enhance the activity of metal oxide for the electrochemical evolution of oxygen.

#### ■ ASSOCIATED CONTENT

**S Supporting Information.** Experimental procedures, detailed calculations of turnover frequencies, SEM, chronoamperometry, and supplementary Raman spectroscopy data. This material is available free of charge via the Internet at <http://pubs.acs.org>.

#### ■ AUTHOR INFORMATION

**Corresponding Author**  
bell@cchem.berkeley.edu

#### ■ ACKNOWLEDGMENT

This work was funded by the Helios Solar Energy Research Center, which is supported by the Director, Office of Science, Office of Basic Energy Sciences of the U.S. Department of Energy under Contract No. DE-AC02-05CH11231. We thank James K. Wu (Material Sciences Division, Lawrence Berkeley National Laboratory) for fabricating the metal targets, Eric Granlund (College of Chemistry, UC Berkeley) for constructing the electrochemical cell, and Grace Y. Lau (Material Sciences Division, Lawrence Berkeley National Laboratory) for assisting in our initial SEM analysis.

#### ■ REFERENCES

- (1) Lewis, N. S.; Nocera, D. G. *Proc. Natl. Acad. Sci. U.S.A.* **2006**, *103*, 15729–15735.
- (2) Turner, J.; Sverdrup, G.; Mann, M. K.; Maness, P. C.; Kroposki, B.; Ghirardi, M.; Evans, R. J.; Blake, D. *Int. J. Hydrogen Energy* **2008**, *32*, 379–407.
- (3) Armaroli, N.; Balzani, V. *Angew. Chem., Int. Ed.* **2007**, *46*, 52–66.
- (4) Jiao, F.; Frei, H. *Angew. Chem., Int. Ed.* **2009**, *48*, 1841–1844.
- (5) Nakagawa, T.; Beasley, C. A.; Murray, R. W. *J. Phys. Chem. C* **2009**, *113*, 12958–12961.
- (6) Esswein, A. J.; McMurdo, M. J.; Ross, P. N.; Bell, A. T.; Tilley, T. D. *J. Phys. Chem. C* **2009**, *113*, 15068–15072.
- (7) Kanan, M. W.; Nocera, D. G. *Science* **2008**, *321*, 1072–1075.
- (8) Singh, R. N.; Hamdani, M.; Koenig, J. F.; Poillat, G.; Gautier, J. L.; Chartier, P. *J. Appl. Electrochem.* **1990**, *20*, 442–446.
- (9) Gorlin, Y.; Jaramillo, T. F. *J. Am. Chem. Soc.* **2010**, *132*, 13612–13614.
- (10) Morris, N. D.; Suzuki, M.; Mallouk, T. E. *J. Phys. Chem. A* **2004**, *108*, 9115–9119.
- (11) Concepcion, J. J.; Tsai, M. K.; Muckerman, J. T.; Meyer, T. J. *J. Am. Chem. Soc.* **2010**, *132*, 1545–1557.
- (12) Hamdani, M.; Singh, R. N.; Chartier, P. *Int. J. Electrochem. Sci.* **2010**, *5*, 556–577.

- (13) Marsan, B.; Fradette, N.; Beaudoin, G. *J. Electrochem. Soc.* **1992**, *139*, 1889–1896.
- (14) (a) Deltombe, E.; Pourbaix, M. *Atlas of Electrochemical Equilibria in Aqueous Solutions*; Pourbaix, M., Ed.; National Association of Corrosion: Houston, TX, 1974; pp 322–329. (b) Chivot, J.; Mendoza, L.; Mansour, C.; Pauporte, T.; Cassir, M. *Corros. Sci.* **2008**, *50*, 62–69.
- (15) Foelske, A.; Strehblow, H. H. *Surf. Interface Anal.* **2002**, *34*, 125–129.
- (16) Bewick, A.; Gutierrez, C.; Larramona, G. *J. Electroanal. Chem.* **1992**, *333*, 165–175.
- (17) Lyons, M. E. G.; Brandon, M. P. *Int. J. Electrochem. Sci.* **2008**, *3*, 1425–1462.
- (18) Castro, E. B.; Gervasi, C. A.; Vilche, J. R. *J. Appl. Electrochem.* **1998**, *28*, 835–841.
- (19) Palmas, S.; Ferrara, F.; Vacca, A.; Mascia, M.; Polcaro, A. M. *Electrochim. Acta* **2007**, *53*, 400–406.
- (20) Singh, R. N.; Koenig, J. F.; Poillerat, G.; Chartier, P. *J. Electrochem. Soc.* **1990**, *137*, 1408–1413.
- (21) Lyons, M. E. G.; Brandon, M. P. *J. Electroanal. Chem.* **2010**, *641*, 119–130.
- (22) McAlpin, J. G.; Surendranath, Y.; Dinca, M.; Stich, T. A.; Stoian, S. A.; Casey, W. H.; Nocera, D. G.; Britt, R. D. *J. Am. Chem. Soc.* **2010**, *132*, 6882–6883.
- (23) Kinoshita, K. *Electrochemical Oxygen Technology*; John Wiley & Sons, Inc.: New York, 1992.
- (24) Lyons, M. E. G.; Brandon, M. P. *Int. J. Electrochem. Sci.* **2008**, *3*, 1386–1424.
- (25) Greeley, J.; Nørskov, J. K. *J. Phys. Chem. C* **2009**, *113*, 4932–4939.
- (26) Kim, B. Y.; Shim, I. B.; Araci, Z. O.; Saavedra, S. S.; Monti, O. L. A.; Armstrong, N. R.; Sahoo, R.; Srivastava, D. N.; Pyun, J. *J. Am. Chem. Soc.* **2010**, *132*, 3234–3235.
- (27) Erts, D.; Ahlberg, E.; Asbjornsson, J.; Olin, H.; Prikulis, J. *Appl. Phys. A: Mater. Sci. Process.* **1998**, *66*, S477–S480.
- (28) Yeo, B. S.; Klaus, S. L.; Ross, P. N.; Mathies, R. A.; Bell, A. T. *ChemPhysChem* **2010**, *11*, 1854–1857.
- (29) da Fonseca, C. N. P.; Depaoli, M. A.; Gorenstein, A. *Adv. Mater.* **1991**, *3*, 553–554.
- (30) Yang, J.; Liu, H. W.; Martens, W. N.; Frost, R. L. *J. Phys. Chem. C* **2010**, *114*, 111–119.
- (31) Tang, C. W.; Wang, C. B.; Chien, S. H. *Thermochim. Acta* **2008**, *473*, 68–73.
- (32) Pauporte, T.; Mendoza, L.; Cassir, M.; Bernard, M. C.; Chivot, J. *J. Electrochem. Soc.* **2005**, *152*, C49–C53.
- (33) Conway, B. E.; Liu, T. C. *Mater. Chem. Phys.* **1989**, *22*, 163–182.
- (34) Simmons, G. W.; Kellerman, E.; Leidheiser, H. *J. Electrochem. Soc.* **1976**, *123*, 1276–1284.
- (35) Simmons, G. W.; Vertes, A.; Varsanyi, M. L.; Leidheiser, H. *J. Electrochem. Soc.* **1979**, *126*, 187–189.
- (36) Kanan, M. W.; Yano, J.; Surendranath, Y.; Dinca, M.; Yachandra, V. K.; Nocera, D. G. *J. Am. Chem. Soc.* **2010**, *132*, 13692–13701.
- (37) Pettinger, B.; Domke, K. F.; Zhang, D.; Schuster, R.; Ertl, G. *Phys. Rev. B* **2007**, *76*, 113409.
- (38) Desilvestro, J.; Weaver, M. J. *J. Electroanal. Chem.* **1986**, *209*, 377–386.
- (39) Boix, A.; Miro, E. E.; Lombardo, E. A.; Banares, M. A.; Mariscal, R.; Fierro, J. L. G. *J. Catal.* **2003**, *217*, 186–194.
- (40) Inaba, M.; Iriyama, Y.; Ogumi, Z.; Todzuka, Y.; Tasaka, A. *J. Raman Spectrosc.* **1997**, *28*, 613–617.
- (41) Tyczkowski, J.; Kapica, R.; Lojewska, J. *Thin Solid Films* **2007**, *515*, 6590–6595.
- (42) Haynes, C. L.; McFarland, A. D.; Van Duyne, R. P. *Anal. Chem.* **2005**, *77*, 338A–346A.
- (43) Yu, K.; Wu, Z. C.; Zhao, Q. R.; Li, B. X.; Xie, Y. *J. Phys. Chem. C* **2008**, *112*, 2244–2247.
- (44) Hammer, B.; Nørskov, J. K. *Adv. Catal.* **2000**, *45*, 71–129.
- (45) Trasatti, S. *Electrochim. Acta* **1984**, *29*, 1503–1512.
- (46) Macdonald, J. J.; Conway, B. E. *Proc. R. Soc. London, Ser. A:* **1962**, *269*, 419–440.
- (47) Matsumoto, Y.; Sato, E. *Mater. Chem. Phys.* **1986**, *14*, 397–426.
- (48) Brossard, L.; Marquis, B. *Int. J. Hydrogen Energy* **1994**, *19*, 231–237.
- (49) Buckley, D. N.; Burke, L. D. *J. Chem. Soc., Faraday Trans. 1* **1976**, *72*, 2431–2440.
- (50) Appleby, A. J.; Crepy, G.; Jacquelin, J. *Int. J. Hydrogen Energy* **1978**, *3*, 21–37.
- (51) Rossmel, J.; Qu, Z. W.; Zhu, H.; Kroes, G. J.; Nørskov, J. K. *J. Electroanal. Chem.* **2007**, *607*, 83–89.